

A multi-task learning framework for carotid plaque segmentation and classification from ultrasound images

Haitao Gan, Ran Zhou, Yanghan Ou, Furong Wang, Xinyao Cheng, Xiaoyan Wu, Aaron Fenster, *Fellow, IEEE*

Abstract—Carotid plaque segmentation and classification play important roles in the treatment of atherosclerosis and assessment for risk of stroke. Although deep learning methods have been used for carotid plaque segmentation and classification, most focused on a single task and ignored the relationship between the segmentation and classification of carotid plaques. Therefore, we propose a multi-task learning framework for ultrasound carotid plaque segmentation and classification, which utilizes a region-weight module (RWM) and a sample-weight module (SWM) to exploit the correlation between these two tasks. The RWM provides a plaque regional prior knowledge to the classification task, while the SWM is designed to learn the categorical sample weight for the segmentation task. A total of 1270 2D ultrasound images of carotid plaques were collected from Zhongnan Hospital (Wuhan, China) for our experiments. The results of the experiments showed that the proposed method can significantly improve the performance compared to existing networks trained for a single task, with an accuracy of 85.82% for classification and a Dice similarity coefficient of 84.92% for segmentation. In the ablation study, the results demonstrated that both the designed RWM and SWM were beneficial in improving the network's performance. Therefore, we believe that the pro-

posed method could be useful for carotid plaque analysis in clinical trials and practice.

Index Terms—Carotid plaque, Multi-task learning, Segmentation, Plaque Classification

I. INTRODUCTION

CARDIOVASCULAR disease (CVD) is the global leading cause of death and disability, and ischemic heart disease and stroke are the primary causes of death among CVD patients [1]. Atherosclerotic plaques can rupture, resulting in thrombus formation and vascular stenosis that can lead to corresponding hemodynamic changes and ischemic cardiovascular events [2]. Because the carotid arteries (CA) have a simple geometry and are easily accessible, they are commonly used to visualize and assess carotid plaques and their potential risk for causing a stroke. Therefore, identifying carotid plaques and assessing them is a critical aspect of treating atherosclerosis and reducing the risk for stroke [3].

Carotid ultrasound is widely used in carotid plaque identification and assessment due to its non-invasive and low-cost characteristics. Over the past decade, researchers have developed various ultrasound biomarkers for the quantification of carotid plaques and showed them to be useful for monitoring changes in the carotid arteries, including intima-media thickness (IMT) [4], total plaque area (TPA) [5], and total plaque volume (TPV) [6]. Furthermore, different types of carotid plaques pose different risks of causing cerebrovascular events such as stroke and TIA. The appearance of carotid plaques in B-mode ultrasound images can be divided into three types: hyperechoic plaque, hypoechoic plaque, and mixed-echoic plaque [7], [8]. Measurement of these ultrasound-based biomarkers requires segmentation of plaque boundaries, and identification of carotid plaque type using classification methods. Thus, segmentation and classification of carotid plaques in ultrasound images are two critical tools in carotid ultrasound image analysis.

Many computer-aided diagnosis algorithms have been proposed for carotid plaque segmentation, which can be divided into two categories: traditional image processing-based methods or deep learning-based approaches. Traditional methods, including level sets, active contour models, snake models, Gaussian mixture models, and geometric priors, have alleviated the manual segmentation process [9]–[11]. However,

This work has been submitted to the IEEE for possible publication. Copyright may be transferred without notice, after which this version may no longer be accessible.

This work was supported by the National Natural Science Foundation of China under grant No. 62201203, the Natural Science Foundation of Hubei Province under grant No. 2021CFB282, the High-level Talents Fund of Hubei University of Technology under grant No. GCRC2020016. (Corresponding author: Ran Zhou.)

Haitao Gan is with the School of Computer Science, the Hubei University of Technology, Wuhan, Hubei, 430068, China (e-mail: htgan01@hbut.edu.cn).

Ran Zhou is with the School of Computer Science, the Hubei University of Technology, Wuhan, Hubei, 430068, China (e-mail: ranzhou@hbut.edu.cn).

Yanghan Ou is with the School of Computer Science, the Hubei University of Technology, Wuhan, Hubei, 430068, China (e-mail: 724334042@qq.com).

Furong Wang is with the Liyuan Hospital, Tongji Medical College, Huazhong University of Science and Technology, Wuhan, Hubei, 430074, China (e-mail: 386600121@qq.com).

Xinyao Cheng is with the Department of Cardiology, Zhongnan Hospital, Wuhan University, Wuhan, Hubei, 430068, China (e-mail: yxcheng@whu.edu.cn).

Xiaoyan Wu is with the Cardiovascular Division, Zhongnan Hospital, Wuhan University, Wuhan, Hubei, 430068, China (e-mail: wuxiaoyan299@aliyun.com).

Aaron Fenster is with the Imaging Research Laboratories, Robarts Research Institute, Western University, London, ON N6A 5B7, Canada (e-mail: afenster@robrats.ca).

these methods are sensitive to contour initialization and image quality, resulting in segmentation inaccuracy and instability that cannot meet the demands of clinical applications. As a result, deep learning-based methods have become the mainstream research direction for carotid plaque segmentation, with most studies focusing on deep learning network structures, loss function design, and post-processing of the segmentation results. Jain et al. developed hybrid deep learning segmentation models (i.e., UNet, UNet+, SegNet, SegNet-UNet, and SegNet-UNet+) for atherosclerotic plaques in the internal carotid artery using B-mode ultrasound images [12]. They further used seven U-series architectures for measuring the area of the plaque far-wall of the common carotid (CCA) and internal carotid arteries (ICA) in B-mode ultrasound images [13]. Mi et al. proposed an MBFF-Net for carotid plaque segmentation in ultrasound images by designing a multi-branch feature fusion module to extract multiple scales and different contexts and exploited the prior information of the carotid artery wall [14]. Li et al. proposed a U-shaped CSWin transformer for carotid artery segmentation in 3D ultrasound images, where hierarchical CSWT modules were used to capture the rich global context information in the 3D image [15]. We also used a U-Net to generate TPA from B-mode carotid ultrasound images [16] [17] and further proposed ensemble learning approaches to reduce segmentation inconsistency, smooth segmentation contours, and improve the accuracy and robustness of plaque segmentation models [18].

Many other works have focused on ultrasound carotid plaque classification. Christodoulou et al. extracted ten different texture feature sets and used the statistical k-nearest neighbor method for atherosclerotic carotid plaque classification [19]. Kyriacou et al. used two classifiers, the Probabilistic Neural Network and the Support Vector Machine (SVM), to classify atherosclerotic carotid plaques into symptomatic or asymptomatic types [20]. Prahl et al. proposed a percentage white feature to classify the echogenicity in carotid plaques [21]. Acharya et al. extracted several grayscale features and input them into an SVM classifier for plaque tissue and classification [22]. Engelen et al. used 3D texture features to predict vascular events from 3D carotid plaque ultrasound images [23]. However, these traditional plaque identification methods rely on feature extraction algorithms that cannot accurately and comprehensively extract carotid plaque features. However, in recent years, researchers have successfully applied deep learning methods to carotid ultrasound image classification. Lekadir et al. used a convolutional neural network (CNN) to identify plaque compositions from carotid ultrasound images [24] and Saba et al. implemented six deep artificial intelligence models for carotid ultrasound plaque characterization using images obtained from a multicenter study [25].

Although deep learning methods have been used for carotid plaque assessment, these methods focused solely on a single segmentation or classification task. However, such methods have limitations: (1) Using two stages for carotid plaque image analysis, the classification performance is sensitive to the accuracy of the prior segmentation task. (2) These methods did not consider the relationship between the segmentation and classification tasks, which could result in under- or

over-segmentation. Therefore, we believe that implementing a multi-task deep learning framework can be advantageous for both the segmentation and classification tasks. This approach has the potential to generate more robust results and could also simplify the processing stream and reduce the computation time. Thus, in this study, we propose a novel multi-task learning framework aimed at facilitating both ultrasound plaque segmentation and classification tasks. The framework incorporates a region-weight module (RWM) and a sample-weight module (SWM) to effectively leverage the correlation between the two tasks. The RWM fuses the segmented probability map with the high-level features of the classification task and is then applied to the feature fusion processing in the classification task. The SWM uses a predicted probability to generate the category sample weights that are embedded in the loss function of the segmentation task. This approach can provide rapid and automatic plaque segmentation and classification with high accuracy and low variability, making it possibly suitable for clinical use.

II. METHODS

The proposed multi-task learning framework leverages the complementary information of carotid plaque segmentation and classification tasks to enhance the overall performance of the system. Figure 1 shows the general framework of our multi-task algorithm, which contains a segmentation task branch and a classification task branch. By segmenting the carotid plaque, the network learns crucial information about the plaque size and shape, enabling the classification branch to concentrate on features in plaque regions while minimizing the influence of irrelevant background information. The classification task provides valuable category information about plaques and integrated this category information into the loss function of the segmentation to improve the segmentation performance of difficult plaque images. The network incorporates two new modules: the region-weight module (RWM) and the sample-weight module (SWM), which mutually enhance the performance of the classification and segmentation tasks. RWM integrates the segmentation probability maps to the feature maps extracted in the classification task, which can make the classification model focus on the plaque region. SWM generates a confidence level to each sample (image) by comparing the predicted and labeled probability distributions of the classification task. This confidence level is used as the sample weight in loss function. The feature extraction layers (layers in red rectangles in Fig. 1) share training weights for the carotid plaque segmentation and classification branches.

A. Network Architecture

U-Net-based network architectures have been widely used in medical image segmentation, and UNet++ is an improvement of U-Net and superior to other U-Net variants [26]. Figure 2 shows the architecture of UNet++, which fuses five convolutional blocks to extract multi-level features. Correspondingly, each convolutional block has a decoding path, except for the first convolutional block. Each decode path uses the upsampling block to convert feature maps of different sizes

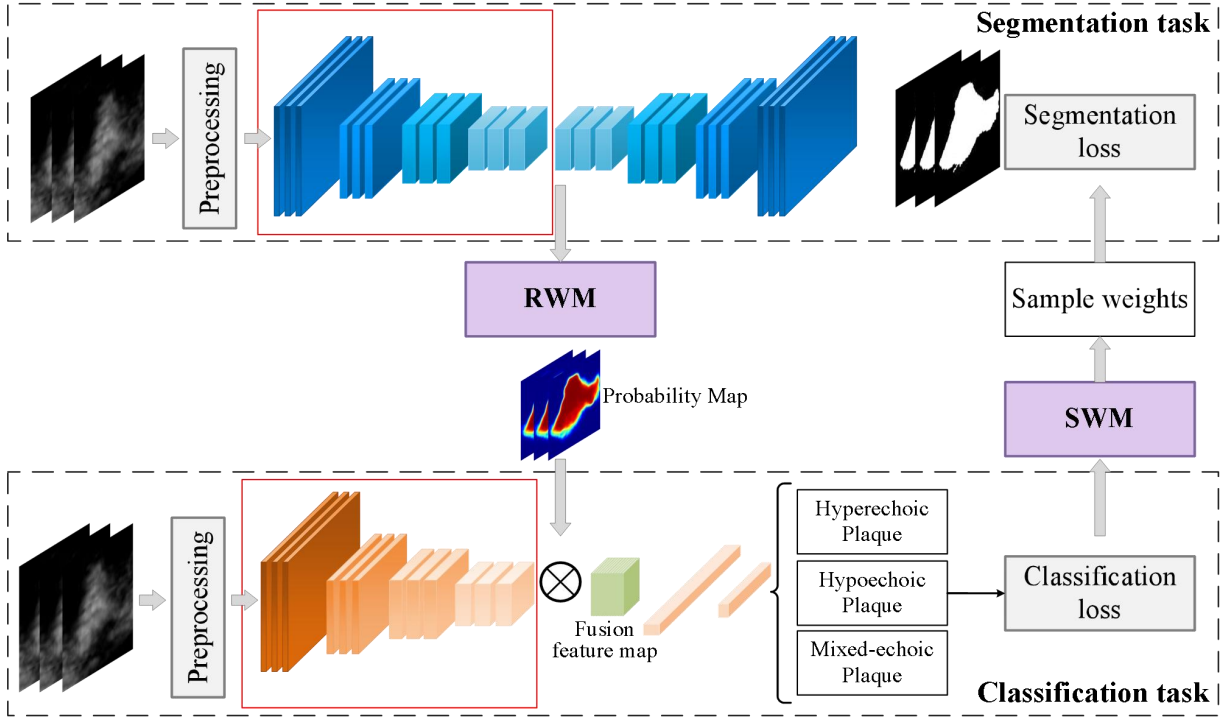


Fig. 1. Framework of our multi-task algorithm including a segmentation task branch and a classification task branch. The feature extraction layers in the segmentation network (red rectangles) and classification network (red rectangles) share weights during training. RWM is a region-weight module and SWM is a sample-weight module.

to the input size and to predict the segmentation mask of the input image. This architecture not only uses skip connections to connect feature maps from the encoder to each decoder path, but also uses skip connections to connect different decoder paths. The architecture enables flexible feature fusion, which helps to alleviate information loss when extracting features and converting images. In our multi-task algorithm, Residual blocks were implemented as the feature extraction layers in UNet++, which are used instead of the convolutional blocks in the backbones of UNet++.

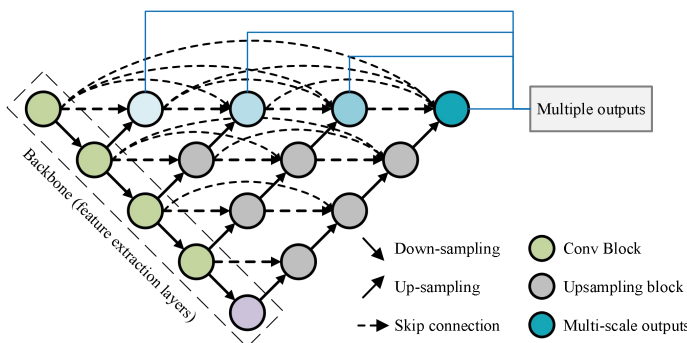


Fig. 2. Architecture of the UNet++ network for the segmentation task. It contains five U-Nets with varying depths that partially share the encoder (backbone), whereas the decoders are densely connected at the same resolution via redesigned skip connections.

The Residual block uses two 1×1 convolution kernels to change the number of channels in the feature map, a 3×3

convolution kernel to extract features, and a short connection to sum the input and output of the convolution kernel [27]. This block alleviates the degradation of the deep neural network, reduces the number of model parameters, and makes the deep neural network easy to be trained.

B. Region-Weight Module (RWM)

To facilitate the classification task, RWM combines the output of UNet++ of the segmentation task to generate the region weights. These weights are then used to fuse the feature maps obtained in the feature extraction layers. Figure 3 shows the detailed architecture of RWM. First, the four outputs of UNet++ are downsampled to the same size as the feature maps obtained in the feature extraction layers. After that, a Softmax function is applied to obtain the probability maps. These probability maps obtained from the segmentation task are used as region-weights in the feature fusion step to improve the classification feature extraction. Each probability map is multiplied by the corresponding position of each channel of the feature map to obtain the region feature map. Finally, the four region feature maps are summed to obtain the fused feature map.

Assuming that the four outputs of UNet++ are $S = \{s_1, s_2, s_3, s_4\}$, the region probability maps ($P = \{p_1, p_2, p_3, p_4\}$) are obtained by

$$p_i = \frac{e^{F_{down}(s_i)}}{\sum_{i=1}^4 e^{F_{down}(s_i)}} \quad (1)$$

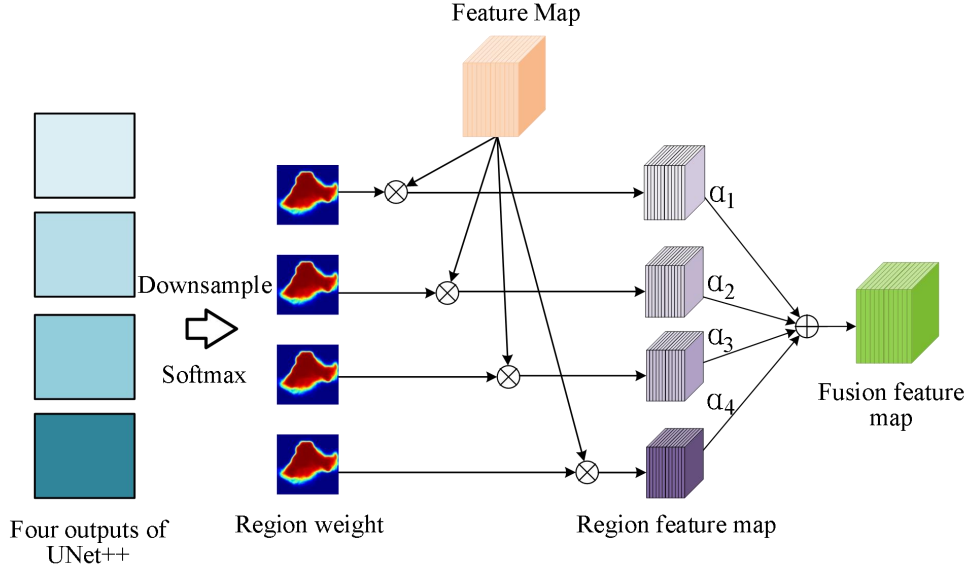


Fig. 3. The details of the RWM. The four outputs of UNet++ are used to obtain four region-weight maps for the region feature fusion task.

where F_{down} is a down-sampling function to make S the same size as the feature maps obtained in the feature extraction layers. The feature maps obtained in the feature extraction layers of the classification task are M . The fusion feature maps (FM) are then formulated as

$$FM = \sum_{i=1}^4 \alpha_i p_i M \quad (2)$$

where α_i is the hyperparameter. The sum of the four hyperparameters equals 1 ($\sum_{i=1}^4 \alpha_i = 1$).

C. Sample-Weight Module (SWM)

SWM uses the results of the classification task to assign a confidence level to each sample, which is then used as the sample-weight in the loss function of the segmentation task. Kullback-Leibler (K-L) Divergence is used to determine the confidence level by calculating the difference between the probability distribution of the classification results and the probability distribution of the labels. Finally, the result of K-L Divergence is used to represent the weights of each sample. Figure 4 shows the implementation details of SWM.

Assuming that y_i denotes the label probability distribution of the i th input sample for classification and $g(x_i; \theta_{cls})$ denotes the probability distribution predicted by the classification network, the confidence level (sample-weight) for the i th sample is obtained by

$$\omega_i = KL(y_i || g(x_i; \theta_{cls})) = \sum_{j=1}^3 y_{i,j} \log\left(\frac{y_{i,j}}{g_j(x_i; \theta_{cls})}\right) \quad (3)$$

For training samples that are incorrectly predicted by the encoder in SWM, the larger the result of K-L Divergence, the smaller the weight of the training samples. This is because a large K-L Divergence indicates that the predicted probability distribution is very different from the ground truth distribution,

which indicates that the model is less confident in its prediction and assigns a smaller weight to the sample. But, if the K-L Divergence is small, it indicates that the predicted distribution is close to the ground truth distribution, and the model is more confident in its prediction, which results in a larger weight for the sample in the loss function.

D. Loss Function

Consider a carotid ultrasound dataset $X = \{(x_i, y_i, z_i) | i \in [1, n], x_i \in \mathbb{R}^{W \times H}, y_i \in \mathbb{R}^{3 \times 1}, z_i \in \mathbb{R}^{2 \times W \times H}\}$, where x_i denotes the i th image, y_i is the class label of the i th image, and z_i is the segmentation label of the i th image, where y_i and z_i are presented in a one-hot format. The number of images in the dataset is n . W and H denote the width and height of carotid ultrasound images, respectively. The weighted cross-entropy loss for segmentation is given by Eq. (4) and the cross-entropy loss for classification is given by Eq. (5).

$$loss_{sc} = -\frac{1}{n} \sum_{i=1}^n \sum_{j=2}^2 w_i y_{i,j} \log f_j(x_i; \theta_{seg}) \quad (4)$$

$$loss_{cc} = -\frac{1}{n} \sum_{i=1}^n \sum_{j=2}^2 z_{i,j} \log g_j(x_i; \theta_{cls}) \quad (5)$$

where w_i is the sample weight generated by SWM for the i th sample, $y_{i,j}$ is the j th element of y_i , f is the classification model's prediction and θ_{seg} is the set of classification network parameters.

Furthermore, we introduced an entropy loss to promote the network to generate a one-hot distribution with a high probability for a single class, instead of using a flat distribution. Consequently, the network will predict results with increased certainty. Through the minimization of the entropy loss, the network can acquire the ability to produce more precise and confident predictions for each input sample. For

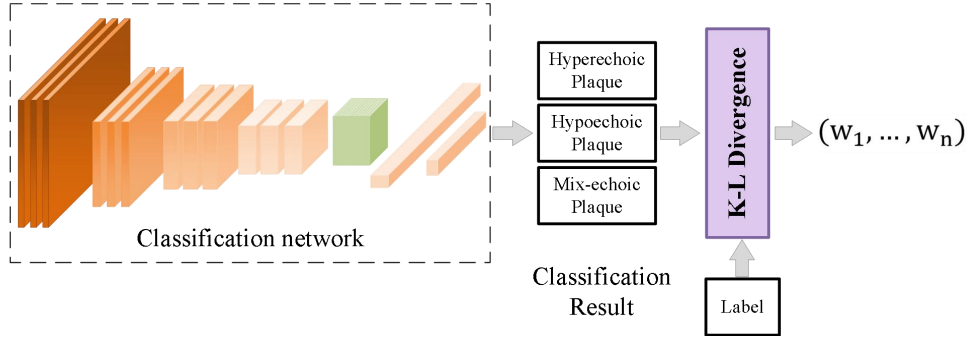


Fig. 4. The details of the RWM. K-L Divergence is used to calculate the confidence of the plaque-type prediction for each sample.

both segmentation and classification tasks, the entropy losses can be defined as

$$loss_{se} = -\frac{1}{n} \sum_{i=1}^n \sum_{j=2}^2 f_j(x_i; \theta_{seg}) \log f_j(x_i; \theta_{seg}) \quad (6)$$

$$loss_{ce} = -\frac{1}{n} \sum_{i=1}^n \sum_{j=2}^2 g_j(x_i; \theta_{cls}) \log g_j(x_i; \theta_{cls}) \quad (7)$$

Finally, the loss function of our multi-task framework is

$$Loss = Loss_{sc} + Loss_{se} + Loss_{cc} + Loss_{ce} \quad (8)$$

E. Evaluation Metrics

To evaluate the performance of our proposed method comprehensively, we employed a set of widely-used metrics to measure both segmentation and classification performance. Specifically, the Dice similarity coefficient (DSC), absolute plaque area difference ($|\Delta PA|$), Hausdorff distance (HD), average symmetric surface distance (ASSD), and Pearson correlation coefficient (PCC) were used to quantify the accuracy of our segmentation results. In addition, we used accuracy (ACC), precision, F1-score, and the Kappa coefficient to assess the classification performance of our algorithm

DSC is used to calculate the similarity between the algorithm segmentation (A) and the manual segmentation (M), as

$$DSC(A, M) = \frac{2|A \cap M|}{(|A| + |M|)} \times 100\% \quad (9)$$

$|\Delta PA|$ is used to calculate the plaque area difference between the algorithm segmentation and manual segmentation as

$$|\Delta PA| = |PA_{alg} - PA_{man}| \quad (10)$$

where PA_{alg} is the algorithm-generated plaque area and PA_{man} is the manually segmented plaque area. ASSD and HD were used to evaluate the distance between the algorithm and manual segmentation contours and are given by:

$$ASSD(A, M) = \frac{1}{2} \left(\frac{1}{|\partial R_A|} \sum_{p \in \partial R_A} d(p, \partial R_M) + \frac{1}{|\partial R_M|} \sum_{p \in \partial R_M} d(p, \partial R_A) \right) \quad (11)$$

$$HD(A, M) = \max \left(\max_{p \in \partial R_A} d(p, \partial R_M), \max_{p \in \partial R_M} d(p, \partial R_A) \right) \quad (12)$$

where ∂R_A is the algorithm segmentation surface and $d(p, \partial R_M)$ is the shortest Euclidean distance from a point p to the manual segmentation surface ∂R_M ; $d(p, \partial R_A)$ is defined in the same manner. The Pearson correlation coefficient (PCC) was used to measure the correlation between the algorithm and manually generated plaque areas.

In classification tasks, in addition to ACC, we also used precision and F1-score to measure the classification performance.

$$F1 - score = \frac{2 \times Precision \times Recall}{Precision + Recall} \quad (13)$$

III. EXPERIMENTS AND RESULTS

A. Data Acquisition

A total of 1270 longitudinal carotid ultrasound images were obtained from Zhongnan Hospital of Wuhan University. The Zhongnan Hospital Institutional Review Board approved the use of the ultrasound data and all patients provided consent. These patients, who had risk factors such as hypertension or hyperlipidemia or had a history of vascular events, underwent ultrasound imaging of their carotid arteries (common, internal, and external). All images were acquired using an Acuson SC2000 (Siemens, Erlangen, Germany) ultrasound system with a 5-12 MHz linear array probe (9L4). Two experienced experts annotated the plaque contours and classified plaques into three categories (i.e., hyperechoic plaque, hypoechoic plaque, and mix-echoic plaque) according to the European Carotid Plaque Study Group criteria.

Before algorithm implementation, we reduced the size of the examined 2D ultrasound images by cropping a region-of-interest around each plaque, as would be done during the clinical examination. The cropped images and manual segmentations were automatically resized to 96×144 matrices as network inputs.

B. Experiment Setting

During the training of the multitask network, the dataset was randomly divided into training, validation, and test sets in the ratio of 6:2:2, resulting in 751, 258 and 261 images in the three sets, respectively. The following parameters were

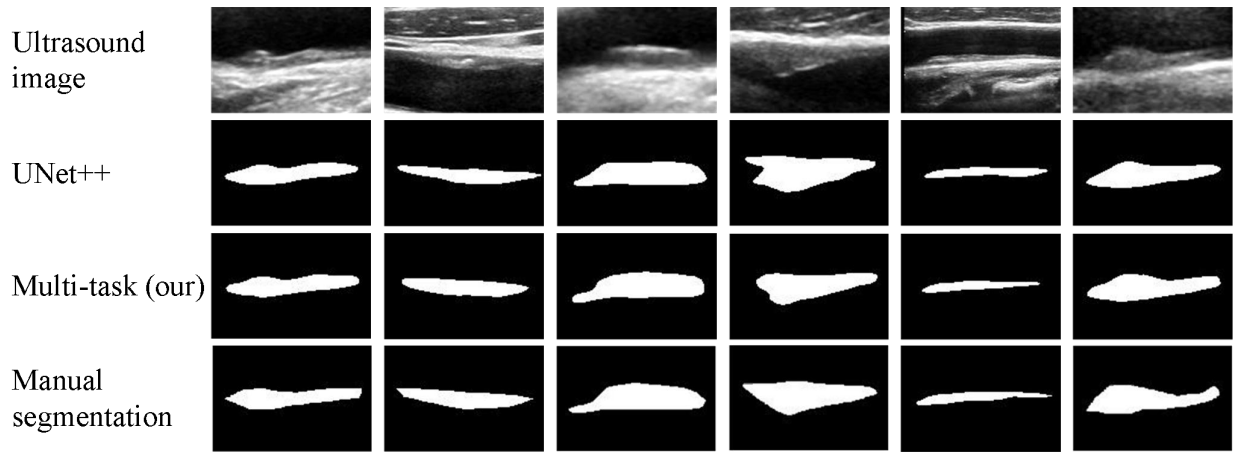


Fig. 5. Comparison of the carotid plaque segmentation results generated by our multi-task and UNet++ models using different backbones. The first row shows the original ultrasound images of the plaques. Row 2 shows the UNet++-generated segmentations. Row 3 shows our multi-task algorithm-generated segmentations. The last row shows manual segmentations.

TABLE I

COMPARISON OF THE EVALUATION METRICS OF OUR ALGORITHM TO A SINGLE SEGMENTATION NETWORK.

Method	DSC (%)	ASSD (mm)	HD (mm)	$ \Delta PA $ (mm ²)	PCC
U-Net	84.05±6.76	0.289±0.173	0.839±0.693	3.995±5.543	0.919±0.011
SegNet	83.66±7.06	0.313±0.203	0.995±0.937	4.325±5.263	0.923±0.008
HRNet	83.06±6.91	0.310±0.205	0.960±0.854	4.252±5.408	0.909±0.030
UNet++	83.95±7.50	0.283±0.188	0.840±0.783	4.292±6.529	0.898±0.012
SegNet-UNet+	84.60±6.30	0.277±0.159	0.844±0.681	3.698±4.974	0.934±0.014
Multi-task (our)	84.92±7.16	0.267±0.164	0.746±0.543	3.599±5.299	0.927±0.013

used for network training: the number of epochs=200, batch size=10, optimizer=ADAM, and learning rate=1e-3. The hyperparameters α_1 , α_2 , α_3 and α_4 in the SWM were set to 0.1, 0.2, 0.3 and 0.4, respectively. All deep learning networks were implemented using Pytorch 1.10.0, CUDA 11.6, and Python 3.8 platforms on an NVIDIA GTX3090 GPU. Ultimately, all experimental results of this paper were obtained from three randomized experiments by setting different random seeds in three repetitions. The segmentation evaluation metric, DSC, ASSD, HD and $|\Delta PA|$, are expressed as mean±SD for the average measurements of all patients and the classification metrics, ACC, Precision, F1-score and Kappa, are presented as mean±SD of results generated by the three randomized experiments.

C. Segmentation Accuracy of the Multi-task Framework

Figure 5 shows representative segmentations of our multi-task approach compared to the baseline UNet++. The multi-task algorithm-generated segmentations outperformed the baseline UNet++ while generating results very close to the manual segmentations.

To evaluate the effectiveness of our proposed multi-task framework, we further compared the performance of our algorithm to networks used for segmentation only, including U-Net [16], SegNet [28], HRNet [29], as well as to the baseline UNet++ [26]. Moreover, our multi-task framework was also compared to an ensemble algorithm (SegNet-UNet+) used for carotid plaque segmentation, which fuses the outputs of SegNet and UNet++ [12]. Table I shows the results of carotid

plaque segmentation. Our multi-task frameworks achieved better performance than the existing single segmentation networks (i.e., U-Net, SegNet, HRNet and UNet++) for all metrics. Compared to baseline UNet++, our multi-task framework increased the DSC over the three different backbones by 1.15%, reduced the ASSD, HD and $|\Delta PA|$ by 5.65%, 11.19% and 16.15%, respectively, and increased the Pearson correlation coefficient from 0.889 to 0.927. Compared to SegNet-UNet+, the multi-task achieved similar performance for most of the evaluation metrics, but the PPC of our algorithm was a little lower than that of SegNet-UNet+.

Figure 6 shows the correlation and Bland-Altman plots comparing the multi-task algorithm and the manually generated plaque areas for 261 carotid ultrasound images and that the correlation is strong and significant with a correlation coefficient of 0.939 ($p < 0.0001$) (Fig. 6(a)) and a small bias of 1.68 mm² with limits agreement from -10.23 to 13.59 mm² (Fig. 6(b)).

D. Classification Accuracy of the Multi-task Framework

To evaluate the classification accuracy of our proposed multi-task framework, we compared the performance of our algorithm to that of different single classification networks, including EfficientNet [30], ResNet [27], DenseNet [31] [31], RepVGG [32] and HRNet [29]. Table II summarizes the carotid plaque classification performance of our multi-task framework and the results from the other networks. Our multi-task frameworks achieved better performance than the existing single classification networks for all metrics. Moreover, our

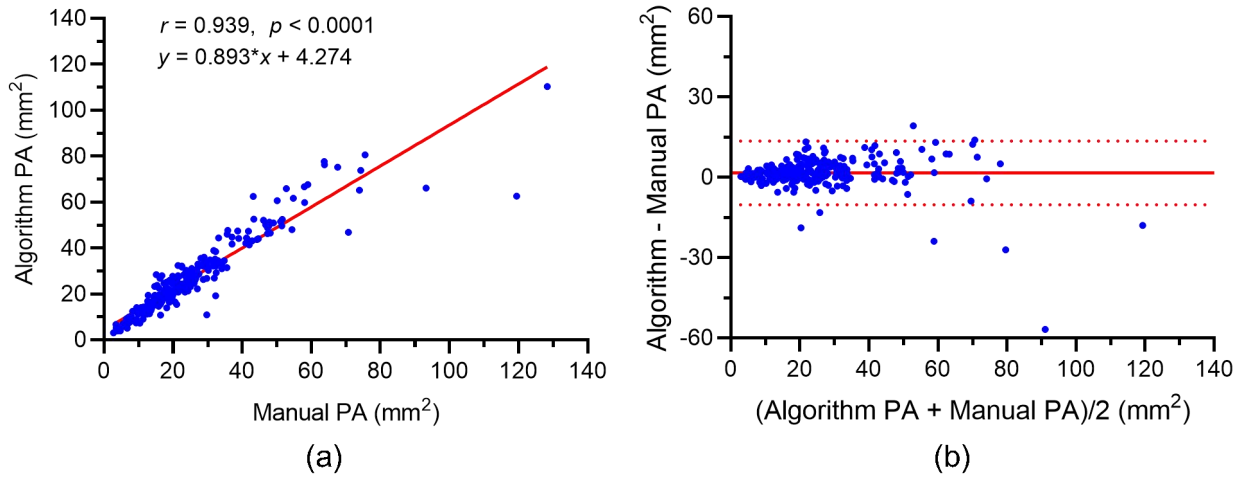


Fig. 6. Relationships of the multi-task (backbone: ResNet) algorithm- and manual- generated plaque area (PA) measurements for $n=261$ carotid plaque images. (a) Linear correlation ($r=0.939$, $p < 0.0001$), and (b) Bland-Altman plot of the two sets of plaque area measurements. The solid red line and the dashed red lines represent the bias (1.684 mm^2) and $\text{mean} \pm 1.96 \text{ SD}$, respectively.

TABLE II
COMPARISON OF THE EVALUATION METRICS OF OUR ALGORITHM TO A SINGLE CLASSIFICATION NETWORK.

Method	ACC (%)	Precision (%)	F1-score	Kappa
EfficientNet	75.09 ± 4.88	75.44 ± 4.73	0.754 ± 0.044	0.609 ± 0.075
ResNet	83.27 ± 0.96	84.08 ± 0.87	0.829 ± 0.001	0.734 ± 0.016
DenseNet	81.61 ± 0.54	81.68 ± 0.19	0.813 ± 0.012	0.710 ± 0.013
RepVGG	77.26 ± 2.22	77.96 ± 2.09	0.760 ± 0.025	0.635 ± 0.037
HRNet	80.07 ± 3.29	81.25 ± 2.78	0.798 ± 0.032	0.682 ± 0.054
Multi-task (our)	85.82 ± 1.36	86.32 ± 1.72	0.854 ± 0.013	0.775 ± 0.021

proposed method increased ACC, Precision, F1-score and Kappa coefficient of baseline by 3.06%, 2.66%, 3.02% and 5.58%, respectively.

In Figure 7 we show the carotid plaque classification performance as confusion matrices of our multi-task model and the baseline UNet++. These results demonstrate that the multi-task approach improves the classification accuracy for all three networks. These results also show that the accuracy of classifying hyperechoic and hypoechoic plaques is higher than that of mixed-echoic plaques.

E. Ablation Experiments

We conducted an ablation study to examine the effectiveness of the RWM and SWM modules. The baseline method (Base) is a general multi-task framework [33] without the use of RWM and SWM. The experimental results are shown in Table III for plaque segmentation and Table IV for plaque classification.

From Table III, we observe that using SWM enhances the DSC, ASSD, and HD of the three backbones by 0.92%, 1.43%, and 7.37%, respectively. We observe that Base+SWM yields significantly better performance in all metrics except $|\Delta PA|$ and PCC, which are very close to the Base results. This suggests that SWM improves the segmentation task by allowing it to focus on misclassified samples with the help of the classification task. Furthermore, by adding the RWM module to the multi-task framework, we observe that Base+SWM+RWM improves all metrics for the three

backbones, except for $|\Delta PA|$, indicating that RWM can also improve the classification performance.

Table IV shows that Base+RWM outperforms Base in almost all metrics, except for the F1-score of ResNet. Specifically, the accuracy, precision, and Kappa are improved by 0.31%, 0.51% and 0.40%, respectively. Base+RWM achieves the same F1-score as 'Base'. These results indicate that the classification task can learn new features from the segmentation task, i.e., the segmentation task can facilitate the classification task. Furthermore, by adding the SWM module to Base+RWM, the performance is improved in all metrics, indicating that SWM is also helpful in the classification task.

F. Computational Time

The mean testing time for a single plaque segmentation and classification by our multi-task framework was 32.09 ± 4.15 ms per image, which is similar to a single segmentation or classification task. This time is sufficiently short to allow plaque analysis immediately after the carotid image acquisition.

IV. DISCUSSION

Accurate segmentation and classification of carotid plaques is crucial for identifying high-risk patients, selecting appropriate treatments, and for monitoring the progression of atherosclerosis. In this study, we propose a new multi-task deep learning framework for carotid ultrasound image analysis that trains a single model to generate both carotid plaque segmentation and plaque types simultaneously. Our experiments

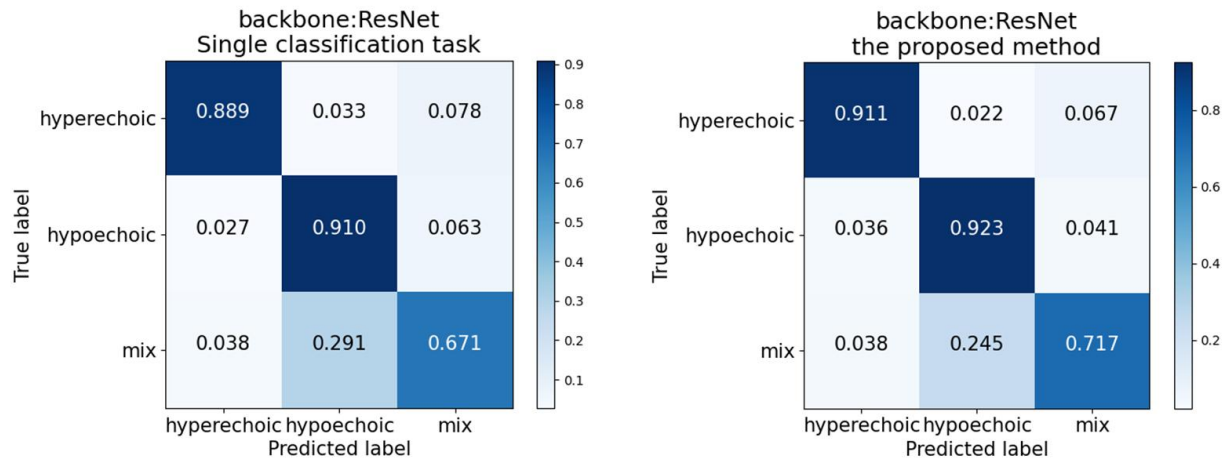


Fig. 7. Confusion matrix comparison of the single classification task with our proposed multi-task method.

TABLE III
ABLATION EXPERIMENT RESULTS FOR SEGMENTATION.

Method	DSC (%)	ASSD (mm)	HD (mm)	$ \Delta PA $ (mm ²)	PCC
Base	83.65±7.17	0.280±0.171	0.868±0.709	3.562±5.303	0.924±0.023
Base+SWM	84.42±7.47	0.276±0.179	0.804±0.639	3.712±5.220	0.922±0.017
Base+SWM+ RWM	84.92±7.16	0.267±0.164	0.746±0.543	3.599±5.299	0.927±0.013

TABLE IV
ABLATION EXPERIMENT RESULTS FOR CLASSIFICATION.

Method	ACC (%)	Precision (%)	F1-score	Kappa
Base	84.29±0.94	84.64±1.05	0.839±0.010	0.751±0.015
Base+RWM	84.55±1.41	85.07±1.24	0.839±0.018	0.754±0.025
Base+SWM + RWM	85.82±1.36	86.32±1.72	0.854±0.013	0.775±0.021

show a strong correlation between our algorithm and manual plaque areas (PA) and excellent accuracies in plaque classification using our multi-task framework. Furthermore, we show the mutually beneficial relationship between the segmentation and classification tasks in improving performance, as well as the efficiency of our algorithm to generate PA and plaque types simultaneously.

The proposed multi-task deep learning framework differs from the previous works that used two-stage model training and existing multi-task algorithms. In particular, the previous carotid ultrasound image analysis methods involved training separate segmentation and classification models and required two stages for testing [12], [25], [34]. However, these methods have several limitations, including segmentation errors leading to decreased classification accuracy and increased training time due to the need for two separate models. The previous multi-task algorithms did not consider the mutually beneficial relationship between the segmentation and classification tasks. For example, Shen et al. developed a multi-task learning method named NDDR-LCS that leverages auxiliary information from ultrasound reports to assist the carotid plaque classification task [35]. In contrast, our method provides a novel framework, aiming at using a single model to accomplish both carotid plaque segmentation and classification tasks. Also, our method incorporated a region-weight module (RWM) and a sample-weight module (SWM) to exploit the relationship between

these two tasks, enabling mutual promotion of the performance of two tasks.

The proposed multi-task algorithm was evaluated on a large dataset with 1270 longitudinal carotid ultrasound images collected in Zhongnan Hospital (Wuhan, China). The manual plaque area (PA) measurements have a mean of 24.03 mm² and range from 1.45 mm² to 187.06 mm² with a majority in the range of 10 mm² to 80 mm². The small areas of these plaques, representing early-stage disease, makes accurate segmentation and classification difficult. Nonetheless, the segmentation task of the developed multi-task algorithm yielded DSC, ASSD, HD and $|\Delta PA|$ in excellent agreement with the manual segmentation results. Compared to the widely used U-Net++ network, our approach achieved better performance by 1.15%, 5.65%, 11.19%, 16.15% for DSC, ASSD, HD, and $|\Delta PA|$, respectively. The algorithm PA measurements were strongly and significantly ($r=0.927$ and $p=0.0001$) correlated with manual measurements. For classification, our algorithm also showed high accuracy and agreement. Compared to the popular classification networks (i.e., EfficientNet, ResNet, DenseNet, RepVGG, and HRNet), our approach achieved the highest performance for ACC, Precision, F1-score, and Kappa coefficient. These results indicate that our approach provided plaque classification performance that are similar to an experienced human operator, possibly making our method usable clinically.

Furthermore, compared to the general multi-task algorithms, our method incorporated RWM and SWM to learn the relationship between plaque segmentation and classification tasks. The ablation results showed that RWM and SWM caused the two tasks to benefit from each other. For the segmentation results as shown in Table III, the DSC, ASSD, HD, $|\Delta PA|$ improved with the help of SWM. For the classification results as shown in Table IV, SWM also showed an increase in specificity, accuracy, precision, and Kappa. This is due to two reasons: (1) RWM integrates the probability map of segmentation results into the high-level features of the classification task, enabling the classification task to learn location information of plaques; (2) SWM utilizes prediction errors as sample weights in the loss function of the segmentation task, enabling the segmentation task to focus on training misclassified samples. These results suggest that the proposed RWM and SWM modules could increase the performance of the multi-task framework.

Although we achieved high algorithm segmentation and classification accuracy, we acknowledge some limitations. We note that the classification accuracy of mixed-echoic plaques is much lower than that of hyperechoic plaques and hypoechoic plaques. This might be because of the complex structure of mixed-echoic plaques, which are more difficult to identify, may result in misclassification of the annotations as mixed-echoic plaques have a higher probability to be misclassified as hyperechoic or hypoechoic plaques. For future work, we will investigate the spatial attention module to make the networks focus on the features within plaques and use sample weights to let the networks bias to the difficult samples. Furthermore, we will also implement this approach to other plaque burden measurements (i.e., Total plaque volume (TPV), Vessel wall volume (VWV)).

V. CONCLUSION

In conclusion, this work is the first to report on the development of a multi-task framework to generate carotid plaque area measurements and plaque types simultaneously, in which the region-weight module and the sample-weight module were developed to exploit the correlation between classification and segmentation. Experimental results show that the proposed approach can effectively improve the accuracy of carotid plaque classification and segmentation, suggesting it may be useful in clinical practice and clinical trials for evaluating new therapies for atherosclerosis.

ACKNOWLEDGMENT

The authors thank the Zhongnan Hospital research team for providing the 2D US images. We also thank the Liyuan Hospital research team for their efforts in manually identifying plaques from carotid ultrasound images.

REFERENCES

- [1] T. Vos, S. S. Lim, C. Abbafati, K. M. Abbas, M. Abbasi, M. Abbasifard, M. Abbasi-Kangevari, H. Abbastabar, F. Abd-Allah, A. Abdelalim *et al.*, "Global burden of 369 diseases and injuries in 204 countries and territories, 1990–2019: a systematic analysis for the global burden of disease study 2019," *The Lancet*, vol. 396, no. 10258, pp. 1204–1222, 2020.
- [2] A. Gisterå and G. K. Hansson, "The immunology of atherosclerosis," *Nature Reviews Nephrology*, vol. 13, no. 6, pp. 368–380, 2017.
- [3] D. Högberg, B. Kragsterman, M. Björck, J. Tjärnström, and A. Wanhainen, "Carotid artery atherosclerosis among 65-year-old Swedish men—a population-based screening study," *European Journal of Vascular and Endovascular Surgery*, vol. 48, no. 1, pp. 5–10, 2014.
- [4] M. L. Bots, A. W. Hoes, P. J. Koudstaal, A. Hofman, and D. E. Grobbee, "Common carotid intima-media thickness and risk of stroke and myocardial infarction: the rotterdam study," *Circulation*, vol. 96, no. 5, pp. 1432–1437, 1997.
- [5] J. D. Spence, M. Eliasziw, M. DiCicco, D. G. Hackam, R. Galil, and T. Lohmann, "Carotid plaque area: a tool for targeting and evaluating vascular preventive therapy," *Stroke*, vol. 33, no. 12, pp. 2916–2922, 2002.
- [6] T. Wannarong, G. Parraga, D. Buchanan, A. Fenster, A. A. House, D. G. Hackam, and J. D. Spence, "Progression of carotid plaque volume predicts cardiovascular events," *Stroke*, vol. 44, no. 7, pp. 1859–1865, 2013.
- [7] A. F. AbuRahma, J. T. Wulu Jr, and B. Crotty, "Carotid plaque ultrasonic heterogeneity and severity of stenosis," *Stroke*, vol. 33, no. 7, pp. 1772–1775, 2002.
- [8] E. Kobayashi, J. Ono, S. Hirai, I. Yamakami, N. Saeki, and A. Yamaura, "Detection of unstable plaques in patients with carotid stenosis using b-mode ultrasonography," *Interventional Neuroradiology*, vol. 6, no. 1, suppl, pp. 165–170, 2000.
- [9] F. Destrempes, J. Meunier, M.-F. Giroux, G. Soulez, and G. Cloutier, "Segmentation of plaques in sequences of ultrasonic b-mode images of carotid arteries based on motion estimation and a bayesian model," *IEEE Transactions on Biomedical Engineering*, vol. 58, no. 8, pp. 2202–2211, 2011.
- [10] C. P. Loizou, S. Petroudi, M. Pantziaris, A. N. Nicolaides, and C. S. Pattichis, "An integrated system for the segmentation of atherosclerotic carotid plaque ultrasound video," *IEEE Transactions on Ultrasonics, Ferroelectrics, and Frequency Control*, vol. 61, no. 1, pp. 86–101, 2014.
- [11] J. Cheng, H. Li, F. Xiao, A. Fenster, X. Zhang, X. He, L. Li, and M. Ding, "Fully automatic plaque segmentation in 3-d carotid ultrasound images," *Ultrasound in Medicine & Biology*, vol. 39, no. 12, pp. 2431–2446, 2013.
- [12] P. K. Jain, N. Sharma, A. A. Giannopoulos, L. Saba, A. Nicolaides, and J. S. Suri, "Hybrid deep learning segmentation models for atherosclerotic plaque in internal carotid artery b-mode ultrasound," *Computers in Biology and Medicine*, vol. 136, p. 104721, 2021.
- [13] P. K. Jain, N. Sharma, M. K. Kalra, A. Johri, L. Saba, and J. S. Suri, "Far wall plaque segmentation and area measurement in common and internal carotid artery ultrasound using u-series architectures: An unseen artificial intelligence paradigm for stroke risk assessment," *Computers in Biology and Medicine*, vol. 149, p. 106017, 2022.
- [14] S. Mi, Q. Bao, Z. Wei, F. Xu, and W. Yang, "Mbf-net: Multi-branch feature fusion network for carotid plaque segmentation in ultrasound," in *Medical Image Computing and Computer Assisted Intervention—MICCAI 2021: 24th International Conference, Strasbourg, France, September 27–October 1, 2021, Proceedings, Part V 24*. Springer, 2021, pp. 313–322.
- [15] Y. Lin, J. Huang, W. Xu, C. Cui, W. Xu, and Z. Li, "Method for carotid artery 3-d ultrasound image segmentation based on cswin transformer," *Ultrasound in Medicine & Biology*, vol. 49, no. 2, pp. 645–656, 2023.
- [16] R. Zhou, M. R. Azarpazhooh, J. D. Spence, S. Hashemi, W. Ma, X. Cheng, H. Gan, M. Ding, and A. Fenster, "Deep learning-based carotid plaque segmentation from b-mode ultrasound images," *Ultrasound in Medicine & Biology*, vol. 47, no. 9, pp. 2723–2733, 2021.
- [17] R. Zhou, F. Guo, M. R. Azarpazhooh, S. Hashemi, X. Cheng, J. D. Spence, M. Ding, and A. Fenster, "Deep learning-based measurement of total plaque area in b-mode ultrasound images," *IEEE Journal of Biomedical and Health Informatics*, vol. 25, no. 8, pp. 2967–2977, 2021.
- [18] R. Zhou, F. Wang, X. Fang, A. Fenster, and H. Gan, "An adaptively weighted ensemble of multiple cnns for carotid ultrasound image segmentation," *Biomedical Signal Processing and Control*, vol. 83, p. 104673, 2023.
- [19] C. I. Christodoulou, C. S. Pattichis, M. Pantziaris, and A. Nicolaides, "Texture-based classification of atherosclerotic carotid plaques," *IEEE transactions on medical imaging*, vol. 22, no. 7, pp. 902–912, 2003.
- [20] E. Kyriacou, M. S. Pattichis, C. S. Pattichis, A. Mavrommatis, C. I. Christodoulou, S. Kakkos, and A. Nicolaides, "Classification of atherosclerotic carotid plaques using morphological analysis on ultrasound images," *Applied Intelligence*, vol. 30, pp. 3–23, 2009.
- [21] U. Prah, P. Holdfeldt, G. Bergström, B. Fagerberg, J. Hulthe, and T. Gustavsson, "Percentage white: a new feature for ultrasound clas-

- sification of plaque echogenicity in carotid artery atherosclerosis,” *Ultrasound in medicine & biology*, vol. 36, no. 2, pp. 218–226, 2010.
- [22] U. R. Acharya, M. M. R. Krishnan, S. V. Sree, J. Sanches, S. Shafique, A. Nicolaidis, L. M. Pedro, and J. S. Suri, “Plaque tissue characterization and classification in ultrasound carotid scans: a paradigm for vascular feature amalgamation,” *IEEE Transactions on Instrumentation and Measurement*, vol. 62, no. 2, pp. 392–400, 2012.
- [23] A. van Engelen, T. Wannarong, G. Parraga, W. J. Niessen, A. Fenster, J. D. Spence, and M. de Bruijne, “Three-dimensional carotid ultrasound plaque texture predicts vascular events,” *Stroke*, vol. 45, no. 9, pp. 2695–2701, 2014.
- [24] K. Lekadir, A. Galimzianova, A. Betriu, M. del Mar Vila, L. Igual, D. L. Rubin, E. Fernández, P. Radeva, and S. Napel, “A convolutional neural network for automatic characterization of plaque composition in carotid ultrasound,” *IEEE Journal of Biomedical and Health Informatics*, vol. 21, no. 1, pp. 48–55, 2016.
- [25] L. Saba, S. S. Sanagala, S. K. Gupta, V. K. Koppula, J. R. Laird, V. Viswanathan, M. J. Sanches, G. D. Kitas, A. M. Johri, N. Sharma *et al.*, “A multicenter study on carotid ultrasound plaque tissue characterization and classification using six deep artificial intelligence models: a stroke application,” *IEEE Transactions on Instrumentation and Measurement*, vol. 70, pp. 1–12, 2021.
- [26] Z. Zhou, M. M. R. Siddiquee, N. Tajbakhsh, and J. Liang, “Unet++: Redesigning skip connections to exploit multiscale features in image segmentation,” *IEEE Transactions on Medical Imaging*, vol. 39, no. 6, pp. 1856–1867, 2019.
- [27] K. He, X. Zhang, S. Ren, and J. Sun, “Deep residual learning for image recognition,” in *Proceedings of the IEEE conference on computer vision and pattern recognition*, 2016, pp. 770–778.
- [28] V. Badrinarayanan, A. Kendall, and R. Cipolla, “Segnet: A deep convolutional encoder-decoder architecture for image segmentation,” *IEEE transactions on pattern analysis and machine intelligence*, vol. 39, no. 12, pp. 2481–2495, 2017.
- [29] J. Wang, K. Sun, T. Cheng, B. Jiang, C. Deng, Y. Zhao, D. Liu, Y. Mu, M. Tan, X. Wang *et al.*, “Deep high-resolution representation learning for visual recognition,” *IEEE transactions on pattern analysis and machine intelligence*, vol. 43, no. 10, pp. 3349–3364, 2020.
- [30] M. Tan and Q. Le, “Efficientnet: Rethinking model scaling for convolutional neural networks,” in *International conference on machine learning*. PMLR, 2019, pp. 6105–6114.
- [31] G. Huang, Z. Liu, L. Van Der Maaten, and K. Q. Weinberger, “Densely connected convolutional networks,” in *Proceedings of the IEEE conference on computer vision and pattern recognition*, 2017, pp. 4700–4708.
- [32] X. Ding, X. Zhang, N. Ma, J. Han, G. Ding, and J. Sun, “Repvgg: Making vgg-style convnets great again,” in *Proceedings of the IEEE/CVF conference on computer vision and pattern recognition*, 2021, pp. 13 733–13 742.
- [33] Y. Ou, H. Gan, R. Zhou, and X. Fang, “An auxiliary learning network for carotid ultrasound image classification,” in *2022 China Automation Congress (CAC)*. IEEE, 2022, pp. 3779–3783.
- [34] S. S. Skandha, S. K. Gupta, L. Saba, V. K. Koppula, A. M. Johri, N. N. Khanna, S. Mavrogeni, J. R. Laird, G. Pareek, M. Miner *et al.*, “3-d optimized classification and characterization artificial intelligence paradigm for cardiovascular/stroke risk stratification using carotid ultrasound-based delineated plaque: Atheromatic™ 2.0,” *Computers in Biology and Medicine*, vol. 125, p. 103958, 2020.
- [35] H. Shen, W. Zhang, H. Wang, G. Ding, and J. Xie, “Nddr-lcs: A multi-task learning method for classification of carotid plaques,” in *2020 IEEE International Conference on Image Processing (ICIP)*. IEEE, 2020, pp. 2461–2465.